Segmentation of Skin Lesions From Digital Images Using Joint Statistical Texture Distinctiveness

Jeffrey Glaister*, *Student Member, IEEE*, Alexander Wong, *Member, IEEE*, and David A. Clausi, *Senior Member, IEEE*

***Abstract*—Melanoma is the deadliest form of skin cancer. Incidence rates of melanoma have been increasing, especially among non-Hispanic white males and females, but survival rates are high if detected early. Due to the costs for dermatologists to screen every patient, there is a need for an automated system to assess a patient's risk of melanoma using images of their skin lesions captured using a standard digital camera. One challenge in implementing such a system is locating the skin lesion in the digital image. A novel texture-based skin lesion segmentation algorithm is proposed. A set of representative texture distributions are learned from an illumination-corrected photograph and a texture distinctiveness metric is calculated for each distribution. Next, regions in the image are classified as normal skin or lesion based on the occurrence of representative texture distributions. The proposed segmentation framework is tested by comparing lesion segmentation results and melanoma classification results to results using other state-of-art algorithms. The proposed framework has higher segmentation accuracy compared to all other tested algorithms.**

***Index Terms*—Melanoma, segmentation, skin cancer, texture.**

I. Introduction

MELANOMA is the most deadly form of skin cancer, with an estimated 76 690 people being diagnosed with melanoma and 9480 people dying of melanoma in the United States in 2013 [1]. In the United States, the lifetime risk of getting melanoma is 1 in 49 [1]. Melanoma accounts for approximately 75% of deaths associated with skin cancer [2]. It is a malignant tumour of the melanocytes and usually occurs on the trunk or lower extremities [3]. Recent trends found that incidence rates for non-Hispanic white males and females were increasing at an annual rate of approximately 3% [4]. If melanoma is detected early, while it is classified at Stage I, the 5-year survival rate is 96% [5]; however, the 5-year survival rate decreases to 5% if the melanoma is in Stage IV [5]. With the rising incidence rates in certain subsets of the general population, it is beneficial to screen for melanoma in order to detect it early. To reduce costs of screening melanoma in the general population, development of automated melanoma screening algorithms have been proposed.

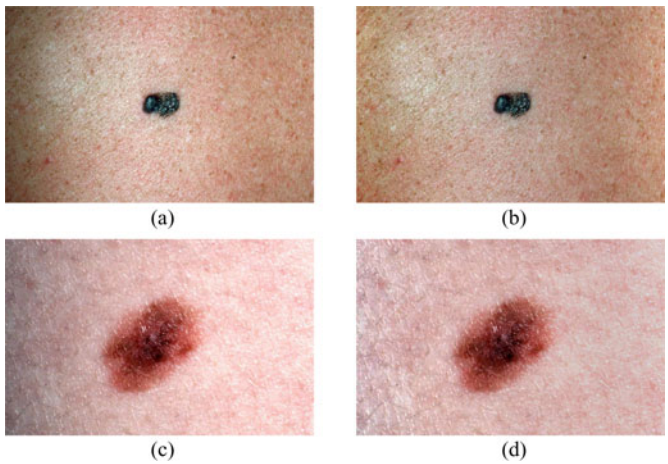

Fig. 1. Uncorrected and corrected skin lesion images. In (a) and (c), examples of the uncorrected skin lesion images are shown. In (b) and (d), the images after being corrected for illumination variation using the MSIM algorithm are shown [14]. Shadows which appear on the left side of the uncorrected images are removed in the corrected images, while the color of the lesion has changed minimally.

Early automated melanoma screening systems assess the risk of melanoma using images acquired via a digital dermatoscope [6]–[9]. A dermatoscope is a special device for dermatologists to use to look at skin lesions that acts as a filter and magnifier. Images acquired through a digital dermatoscope are referred to as dermoscopy images and have relatively low levels of noise and consistent background illumination. Optional preprocessing algorithms applied to dermatological images include normalizing or enhancing image colors [10]. However, requiring dermatologists to have a dermatoscope impedes the adoption of these systems as only 48% of practicing dermatologists use dermatoscopes [11]. The most common reasons against using the dermatoscope include a lack of training or interest. Recent work with automated melanoma screening algorithms tries to adapt the algorithms to analyze images taken by a standard digital camera [12], [13]. Examples of digital images of melanoma are shown in Fig. 1(a) and (c). There is a need for a segmentation algorithm designed specifically for digital images of skin lesions.

Before extracting features from the skin lesion and classifying the lesion as malignant or benign, the location of the lesion border must be identified using a segmentation algorithm. Finding an accurate estimate of the lesion border is important because of the types of features used for classification. One common set

Manuscript received October 22, 2013; revised December 13, 2013; accepted December 21, 2013. Date of publication January 2, 2014; date of current version March 17, 2014. This work was supported by Agfa Healthcare Inc., Ontario Ministry of Research and Innovation, Ontario Centres of Excellence, the Natural Sciences and Engineering Research Council of Canada, and the Canada Research Chairs program. *Asterisk indicates corresponding author.*

*J. Glaister is with the Image Analysis and Communications Lab, Department of Electrical and Computer Engineering, Johns Hopkins University, Baltimore, MD 21218 USA (e-mail: jglaist1@jhu.edu).

A. Wong and D. A. Clausi are with the Vision and Image Processing Lab, Department of Systems Design, University of Waterloo, ON N2L 3G1, Canada (e-mail: a28wong@uwaterloo.ca; dclausi@uwaterloo.ca).

Color versions of one or more of the figures in this paper are available online at http://ieeexplore.ieee.org.

Digital Object Identifier 10.1109/TBME.2013.2297622

of features is the ABCD scale: asymmetry, border irregularity, color variegation, and diameter [15]. In particular, metrics that measure border irregularity may depend heavily on the accuracy of the estimated lesion border. Therefore, it is important that the skin lesion segmentation algorithm is accurate, as the resulting segmentation is used as an input to feature extraction and melanoma classification algorithms.

Many segmentation algorithms have been proposed to locate skin lesion in images automatically. The majority of proposed segmentation algorithms are only applicable to dermoscopy images, which has better contrast between the lesion and surrounding skin area for certain types of lesions [16]. A recent summary by Celebi *et al.* [16] reviews the existing segmentation algorithms for dermoscopy images. Algorithms compared in the summary [16] include using simple thresholding, active contours [17], and region merging [18]. The majority of algorithms only use features derived from pixel color to drive the segmentation. This includes the blue channel from the RGB color space, the luminance channel from the CIELUV or CIELAB color spaces, or an orthogonal transform applied to the color channels. However, to accurately segment lesions with fuzzy edges is difficult when relying solely on color features.

Segmenting digital photographs of skin lesions is a more difficult problem due to illumination variation. Special segmentation algorithms are required to take into account illumination variation, which causes shadows and bright areas to appear throughout the photograph. Hance *et al.* [19] explored different algorithms, including thresholding, active contours and split-and-merge, and modified them to be usable on lesion photographs. For example, the thresholding algorithm has to be modified to account for bright areas where there is reflection of the camera's flash.

Four separate algorithms by Cavalcanti *et al.* include a preprocessing step which corrects for illumination variation before applying a thresholding [12], [20], [21] or level-set segmentation algorithm [22]. Thresholding is performed on single color channels [21], multiple color channels [20], or a set of channels derived using principal component analysis (PCA) and other processing steps [12]. Without the preprocessing step correcting for illumination variation, these algorithms tend to identify areas with shadows as part of the skin lesion. The proposed algorithm incorporates this idea and includes a multistage illumination modelling [14] preprocessing step to correct shadows and bright spots caused by illumination variation. Examples of corrected images are shown in Fig. 1(b) and (d). In both examples, shadows that appeared on the left side of the uncorrected images have been removed. The corrected images are used as the input to the segmentation algorithm.

Most segmentation algorithms for dermatological images or photographs use color information, either in a single channel or across three color channels, to find the lesion. Another approach to find skin lesions is to incorporate textural information, because normal skin and lesion areas have different textures. Textures include smoothness, roughness, or the presence of ridges, bumps or other deformations and are visible by variation in pixel intensities in an area [23]. Features and measurements of a texture in an image are extracted and textures from different regions are compared. Stoecker *et al.* [24] analyzed texture in skin images using basic statistical approaches, such as the gray-level cooccurrence matrix. They found that texture analysis could accurately find regions with a smooth texture and that texture analysis is applicable to segmentation and classification of dermatological images.

Texture-based segmentation algorithms have been applied to dermoscopy images. Proposed textural lesion segmentation algorithms include using gray-level cooccurrence matrix [25], first-order region statistics [26], and Markov random field models [27]. The algorithm proposed by Xu *et al.* [28] learns a model of the normal skin texture using pixels in the four corners of the image, which is later used to find the lesion. Hwang and Celebi [29] use Gabor filters to extract texture features and use a g-means clustering approach for segmenting the lesion.

In this paper, we propose a segmentation algorithm based on texture distinctiveness (TD) to locate skin lesions in photographs. This algorithm is referred to as the TD lesion segmentation (TDLS) algorithm. The main contributions are the introduction of a joint statistical TD metric and a texture-based region classification algorithm. TD captures the dissimilarity between learned representative texture distributions. In Section II, the process of learning the sparse texture model and calculating a metric to measure TD is described. As part of this contribution, we introduce the use of joint statistical information to characterize skin and lesion textures as representative texture distributions. In Section III, regions in the image are classified as being part of the lesion or normal skin. This region classification algorithm incorporates the texture information captured by the TD metric. Implementation details are provided in Section IV. Experimental results are shown in Section V and conclusions are drawn in Section VI.

II. Texture Distinctiveness

The TDLS algorithm consists of two main steps. First, a set of sparse texture distributions that represent skin and lesion textures are learned. A TD metric is calculated to measure the dissimilarity of a texture distribution from all other texture distributions. Second, the TD metric is used to classify regions in the image as part of the skin class or lesion class. In this section, the first step is described in detail and Fig. 2 illustrates the overall process to learn the representative texture distributions and calculate the TD metric.

Existing sparse texture algorithms use sparse texture models for segmentation or classification of images with different texture patterns. Sparse texture models find a small number of texture representations, such as texture patches, to characterize an entire image [30]. Sparse texture models learn important local texture details present in an image. Using a sparse texture model allows the image to be stored efficiently and allows for efficient computation of algorithms that involve textures from the image. There are many ways to learn the model, including clustering or by formulating the problem as an optimization problem [31]. A common method to learn a sparse texture model is by employing a dictionary-learning algorithm [30], where a set of texture patches that can best match details in the original

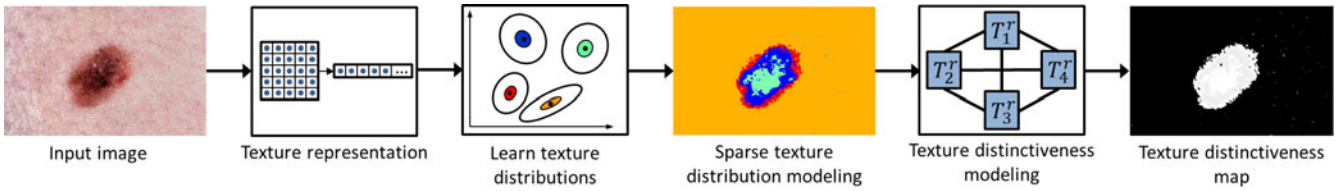

Fig. 2. Algorithm flowchart displaying the steps to learn the representative texture distributions and calculate the TD metric.

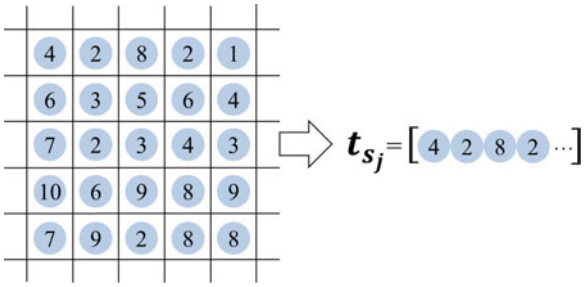

Fig. 3. Extracting a texture vector. For images with multiple channels, a separate vector is obtained for each channel and concatenated sequentially.

image is learned. We propose incorporating probabilistic information to learn sparse texture distributions, rather than texture models. To learn whether each texture distribution belongs to the skin or lesion class, a TD metric is formulated.

A. Representative Texture Distributions

An existing sparse texture model algorithm [32] is modified to find representative sparse texture distributions from the input photograph. Our proposed sparse texture model algorithm incorporates statistical information. The advantage of using a joint probabilistic sparse model is that the sparse texture distributions can model both local and global texture characteristics.

To learn the sparse texture model, a local texture vector is obtained for each pixel in the image. The input image has been corrected for illumination variation, contains $N \times M$ pixels and each pixel has a channels. The texture vector contains pixels in a neighborhood of size n centered on the pixel of interest. Let s be a pixel location (x, y) in the photograph. Then, the vector $\boldsymbol{t}_s$ represents the $n \times n \times a$ texture patch centered at pixel s. The process of extracting the texture vector for a pixel in a single channel is illustrated in Fig. 3. To account for edge pixels, the borders of image are padded.

In the case of a multiple channels, $\boldsymbol{t}_{A,s}$ is the texture patch centered at pixel s and corresponding to channel A. The texture vector is constructed by concatenating each $\boldsymbol{t}_{A,s}$ corresponding to the same pixel across all channels. For example, if the color image contains three channels $\{R, G, B\}$ for each pixel, three texture vectors, $\boldsymbol{t}_{R,s}, \boldsymbol{t}_{G,s}$, and $\boldsymbol{t}_{B,s}$, are extracted and concatenated such that $\boldsymbol{t}_s = [\boldsymbol{t}_{R,s}, t_{G,s}, t_{B,s}]$. After extracting the set of texture vectors for an image, we have a set of $N \times M$ texture vectors is extracted, with each vector of size $n \times n \times a$:

$$\mathcal{T} = \{\boldsymbol{t}_{s_j} | 1 \leq j \leq N \times M\}. \tag{1}$$

Using the set of all texture vectors extracted from an image, we find a set of representative texture distributions. By characterizing the sparse model as a set of distributions, we can capture both local and global characteristics in the image. The texture distributions are able to capture the commonly occurring texture patterns found in lesion and normal skin regions. The kth representative texture distribution is defined as T_k^r. By using a small set $\mathcal{T}^r$ comprised of K representative texture distributions instead of using all the local texture vectors, the computational complexity and memory requirements are reduced,

$$\mathcal{T}^r = \{T_k^r | 1 \leq k \leq K\}. \tag{2}$$

Each texture vector belongs to a single representative texture distribution, which best corresponds with that texture vector. All parameters needed to characterize the kth texture distribution are contained in θ_k. Each distribution has its own distinct set of parameters. A mixture model is used to represent the set of texture distributions associated with the input photograph. Texture distributions are chosen to maximize the log-likelihood of the mixture model,

$$\hat{\mathcal{T}}^r = \arg\max_{\mathcal{T}^r} \sum_{k=1}^{K} \sum_{\boldsymbol{t}_{s_j} \in C_k} \log\left(\mathrm{P}(\boldsymbol{t}_{s_j} | \mathrm{T}_k^r)\right). \tag{3}$$

To find the representative texture distributions and the sets of texture vectors corresponding to each representative distribution, an unsupervised clustering algorithm is used. The set C_k is comprised of the texture vectors corresponding to texture distribution T_k^r. Implementation details are given in Section IV. A Gaussian distribution is assumed, so θ_k contains the two required parameters to define a multivariate Gaussian distribution. The mean and covariance of the kth texture distribution are represented by $\boldsymbol{t}_k^r$ and Σ_k, respectively. $P(\boldsymbol{t}_{s_j} | T_k^r)$ is the probability of the jth texture vector given the parameters of the kth texture distribution. The parameters of the texture distributions are chosen to maximize the log-likelihood in (3).

Examples of photographs where pixels associated with a set of five representative texture distributions are shown in Fig. 4. Each solid color in Fig. 4(b) and (e) represents pixels belonging to the same representative texture distribution. In Fig. 4(b), the lesion is represented by texture distribution associated with dark blue and in Fig. 4(e), the lesion is represented by texture distributions associated with dark blue and light green.

B. TD Metric

A TD metric is formulated using the learned sparse texture model. Since we are only interested in two classes, normal skin and lesion, but have learned many texture distributions, multiple texture distributions must represent the same class. To measure similarity of two texture distributions, we first measure the

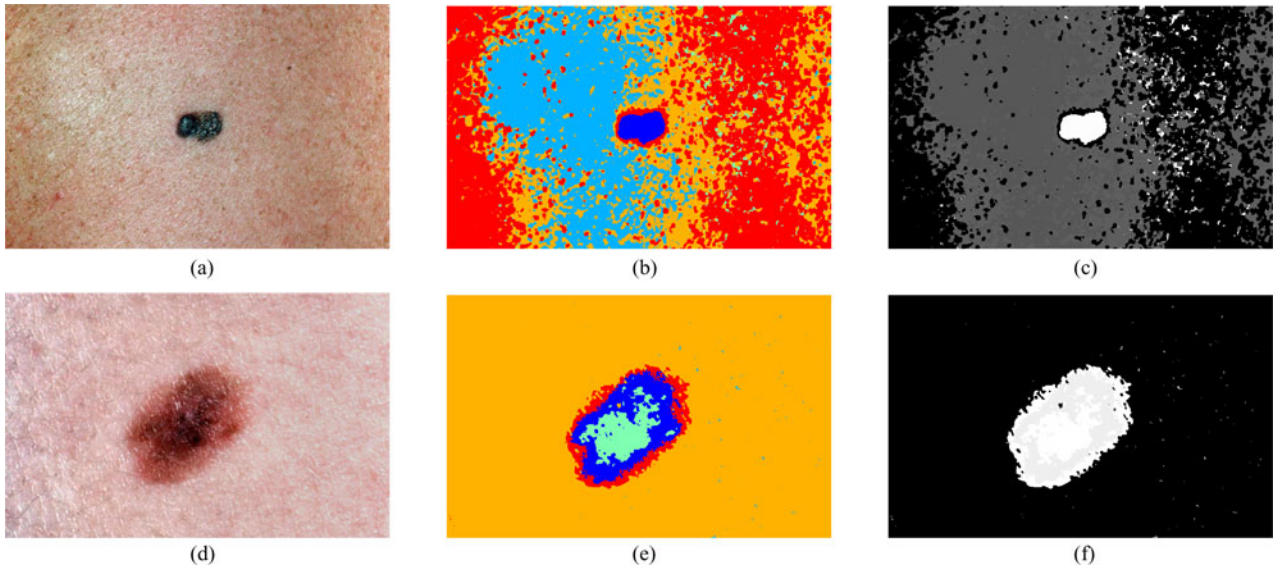

Fig. 4. Map of representative texture distributions. In (a) and (d), the original images are shown. In (b) and (e), five representative texture distributions have been learned and each pixel in the image is replaced by one of five colors, depending on which texture distribution that pixel is associated with. In (c) and (f), maps of the texture distinctive metric are constructed. The pixel intensities in (c) and (f) depend on the TD of the texture distribution associated with each pixel.

probability that the mean of one texture distribution is a realization of the mean of the other texture distribution, which is defined as $l_{j,k}$ in (4). Because we assume that the texture distributions are Gaussian, $\boldsymbol{t}_j^r$ and Σ_j are the mean and covariance of distribution T_j^r. The metric $l_{j,k}$ is asymmetric, because when comparing most pairs of distributions, $\Sigma_i \neq \Sigma_j$. The measure of similarity $L_{j,k}$ given in (5) is the average of $l_{j,k}$ and $l_{k,j}$. After $L_{j,k}$ has been calculated for each pair of texture distributions, they are normalized to be between 0 and 1,

$$l_{j,k} = \frac{1}{\sqrt{(2\pi)^{n\times n\times a}|\Sigma_j|}} \exp\left(-\frac{1}{2}(\boldsymbol{t}_j^r - \boldsymbol{t}_k^r)^T \Sigma_j^{-1}(\boldsymbol{t}_j^r - \boldsymbol{t}_k^r)\right) \quad (4)$$

$$L_{j,k} = \frac{1}{2}\left(l_{j,k} + l_{j,k}\right). \quad (5)$$

We are interested in finding distinct texture distributions. For example, lesion texture distributions are both dissimilar from the normal skin texture distributions and also from other texture distributions, due to color variegation and textural patterns found in skin lesions. The probability that a texture distribution is distinct from another texture distribution is given by $d_{j,k}$:

$$d_{j,k} = 1 - L_{j,k}. \quad (6)$$

Using the texture distributions and probabilities of distinctiveness, a weighted graphical model can be constructed to characterize all pair-wise relationships. The graphical model is defined as $G = \{\mathrm{V}, \mathrm{E}\}$. V represents the set of vertices for the graphical model, which are the texture distributions associated with each pixel in the image. E represents the set of edges between every pair of texture distributions, which are given a weight based on the probability of distinctiveness, $d_{j,k}$.

A TD metric D_j is used to capture the dissimilarity of texture distribution T_j^r from other texture distributions. The metric is defined in (7) and measures the expected distinctiveness of T_j^r given the photograph I, where $P(T_k^r|I)$ is the probability of occurrence of a pixel being associated with a texture distribution T_k^r. $P(T_k^r|I)$ is estimated using the histogram of the number of pixels associated with each texture distribution across the entire image,

$$D_j = \sum_{k=1}^{K} d_{j,k} P(T_k^r|I). \quad (7)$$

In the case of normal skin texture distributions, the dissimilarity of one skin texture distribution from other skin texture distributions is very small. The TD metric for skin texture distributions is small overall. Lesion texture distributions are dissimilar from other skin and lesion texture distributions, so the textural distinctiveness metric is large.

Fig. 4(c) and (f) give illustrative examples of the TD metric corresponding to each pixel in the images. A brighter pixel corresponds to a higher TD metric. In both figures, the lesion is predominately white, meaning that the lesion texture distributions have higher TD metrics, as expected. In Fig. 4(f), there are two texture distributions that correspond to the lesion class and have high TD. However, in Fig. 4(c), some normal skin pixels to the right of the lesion also have high TD. This can occur when there are unique texture patterns in normal skin areas. This commonly occurs, motivating the region classification step of the TDLS algorithm. The region classification step allows the algorithm to be more robust and minimize misclassification of pixels.

III. Region Classification

The second main step in the TDLS algorithm is to find and classify regions in the input image as being part of the lesion based on the sparse texture distributions and their associated TD metric. First, the image is oversegmented, which results in the image being divided into a large number of regions. Next, each region is independently classified as representing normal skin

or lesion based on the textural contents of that region. Finally, postprocessing steps refine the lesion segmentation.

A. Initial Regions

The corrected lesion image is divided into a large number of regions. This initial oversegmentation step is incorporated to increase the TDLS algorithm's robustness to noise. Furthermore, it allows for the use of an efficient and fast classification algorithm to find which regions belong to the skin or lesion class. The initial oversegmentation algorithm is adapted from the statistical region merging (SRM) [33] algorithm. The main difference is that the SRM algorithm uses the image in the RGB color space, while the TDLS algorithm converts the photograph to the XYZ color space, as mentioned in Section IV. The advantages of using the SRM algorithm as the initial oversegmentation algorithm are that it directly takes into account pixel location, is simple and is computationally efficient.

SRM contains two main steps: a sorting step and a merging step. SRM sorts pixels in an image to determine the order in which pixels are compared, and then merges pairs of pixels into regions based on their similarity. A four-connected graph is constructed so that each pixel in the photograph is connected with its neighbors. The pixels are sorted based on their similarity with their neighboring pixel. Both horizontal and vertical neighboring pixels are considered when sorting the pixels. The merging predicate determines whether two regions are merged together, based on pixel intensities. The predicate depends on the difference between average pixel intensity for each channel for the two regions. Furthermore, it depends on the number of pixels in the regions. It includes a tunable parameter Q to change the likelihood that two regions are merged. The parameter Q is set to 128 following experimental testing. Additional details are available in the paper by Nock and Nielson [33].

The result of the initial oversegmentation step is a map of several regions which correspond to the normal skin or lesion classes. To reduce the number of regions, all segments that touch the edges of the photograph are merged into a single region. This is based on the assumption that the lesion is not touching the edges of the photograph, which is reasonable for situations where the photographs are captured in controlled, clinical environments. As such, regions touching the edges are all likely to be part of the normal skin class.

B. Distinctiveness-based Segment Classification

Following the initial oversegmentation step, each region must be classified as belonging to the normal skin class or lesion class based on a criterion. The classification step is illustrated in (8), where y is the resulting segmentation map. Each element in y is either 1 (lesion) or 0 (normal skin), depending on the classification results for that element's corresponding region. The threshold is denoted by τ and it represents the decision boundary between the normal skin and lesion class. The feature used to discriminate between the two classes is the regional textural distinctiveness metric $\mathcal{D}_R$. This metric is based on the TD across a region,

$$y(R) = \begin{cases} 1, & \text{if } \mathcal{D}_R \geq \tau \text{ (lesion)} \\ 0, & \text{otherwise (normal skin).} \end{cases} \tag{8}$$

From Section II-A, each pixel in the input photograph is associated with a texture distribution. A TD metric D is calculated for each texture distribution based on the probability of it being similar to other texture distributions. This information is combined with the contents of each region to determine a regional TD metric, $\mathcal{D}_R$. $\mathcal{D}_R$ represents the average TD across region R (9), where $P(T_j^r|R)$ is the probability of a pixel being associated with the jth texture distribution in region R. Again, $P(T_j^r|R)$ is estimated using the histogram of the number of pixels associated with each texture distribution across the region R,

$$\mathcal{D}_R = \sum_{j=1}^{K} D_j P(T_j^r|R). \tag{9}$$

Finally, a threshold τ is defined to divide the set of representative texture distributions into two classes, normal skin and lesion, and is also based on the TD metrics. There are many ways to find two classes from a one-dimensional set of features. In the TDLS algorithm, the threshold is found that divides the set of texture distributions into two classes such that the total intraclass variance of the TD metric for each class is minimized as

$$\tau = \arg\min_{\tau} \left(\sigma^2_{C_1(\tau)} P\left(T^r|C_1(\tau)\right) + \sigma^2_{C_2(\tau)} P\left(T^r|C_2(\tau)\right) \right). \tag{10}$$

The threshold τ is used to divide the set of texture distributions into two classes $C_1(\tau)$ and $C_2(\tau)$. The classes depend directly on τ because if the distinctiveness metric of the associated texture distribution is above τ, that texture distribution is in class $C_1(\tau)$. Likewise, if it is below τ, it is in class $C_2(\tau)$. The probability that a texture distribution is in the class C for a given τ is $P(T^r|C(\tau))$ and the variance of the TD based on the elements in the class is $\sigma_{C(\tau)}$. This threshold is known as the Otsu's threshold [34].

C. Segmentation Refinement

After the regions are classified as being normal skin or lesion, the following postprocessing steps are applied to refine the lesion border: morphological dilation and region selection.

First, the morphological dilation operator is applied to fill holes and smooth the border. Morphological dilation is a process that expands binary masks to fill small holes [35]. The shape and amount that the binary mask is expanded is controlled by a structuring element, which is a disc with a radius of 5 pixels in the TDLS algorithm.

Next, since multiple noncontiguous regions may have been identified as part of the lesion class, the number of regions is reduced to one. While it is possible to have multiple lesions in a single image, it is necessary to reduce the number of lesions for the feature extraction step. Features proposed by both Celebi *et al.* [6] and Cavalcanti and Scharcanski [12] assume that only a single lesion is being analyzed in the image. To eliminate the small regions, the number of pixels in each contiguous region

is counted. The contiguous region with the largest number of pixels is assumed to correspond to the lesion class and any other regions are converted to the normal skin class. This gives the final lesion segmentation.

IV. Implementation Details

A. Color Space

In the implementation of the TDLS algorithm, the photograph is in the RGB domain and has three channels ($a = 3$). However, the algorithm can be generalized and expanded to take into account multi- or hyperspectral images of a skin lesion, where a is much greater than three channels.

For standard digital images, we convert the image to the XYZ color space to find texture distributions and during the initial oversegmentation. Work by Terrillon *et al.* [36] found that the XYZ color space proved to be an efficient color space in which to segment the skin region of human faces. This color space is designed to better model color perception and reduce correlation between the XYZ channels, compared to the standard RGB color space.

B. Learning Representative Texture Distributions

In this implementation, a two-step clustering algorithm is used. First, a *k*-means clustering algorithm is run, which is followed by learning a finite mixture model. *K*-means clustering is used as an initial step to increase the robustness and to speed up the number of iterations required for the finite mixture model to converge. *K*-means clustering finds K clusters of texture data points that minimizes the sum of squared error between cluster members and the cluster mean. The optimization function for *k*-means clustering is shown in (11), where C_k is the kth set of texture vectors, and $\boldsymbol{\mu}_k$ is defined as the mean vector for the kth set. Implementation details for *k*-means clustering can be found in [37]. Here, the initial cluster means are randomly assigned. Other methods to initialize the clusters could be used to decrease the sensitivity of *k*-means clustering to initial cluster placement [38],

$$\hat{C} = \arg\min_{C} \sum_{k=1}^{K} \sum_{\boldsymbol{t}_{s_j} \in C_k} \|\boldsymbol{t}_{s_j} - \boldsymbol{\mu}_k\|^2. \tag{11}$$

One limitation with *k*-means clustering is that it does not take into account any probabilistic information. Therefore, the second step is to apply finite mixture model clustering. To fit the finite mixture model, the model parameters in the set Θ are found to maximize the log-likelihood function shown in (12).

In this implementation, a Gaussian distribution is assumed for all clusters and the model parameters are the distribution mean μ and distribution covariance Σ. Θ also contains the parameter α, which is the mixing proportion. No closed form solution exists for (12) in general, so an expectation-maximization iterative algorithm is used [39]. The expectation-maximization algorithm is initialized using cluster means, covariances, and mixing proportions based on the results of the *k*-means clustering,

$$\hat{\Theta} = \arg\min_{\Theta} \sum_{j=1}^{n} \sum_{k=1}^{K} \log\left(\alpha_i P(\boldsymbol{t}_{s_j} | \boldsymbol{\mu}_k, \Sigma_k)\right)$$

$$\text{where } \sum_{k=1}^{K} \alpha_k = 1 \text{ and}$$

$$\Theta = \{\boldsymbol{\mu}_1, \boldsymbol{\mu}_2, \ldots, \boldsymbol{\mu}_K, \Sigma_1, \Sigma_2, \ldots, \Sigma_K, \alpha_1, \alpha_2, \ldots, \alpha_K\}. \tag{12}$$

Expectation-maximization is an iterative algorithm. The initial parameters for the Gaussian mixture model are obtained from the results of the *k*-means clustering. That is, the initial Gaussian means are equal to the *k*-means cluster means:

$$\boldsymbol{\mu}_k = \boldsymbol{\mu}_{C_k} \tag{13}$$

and the distribution covariances and mixing proportions are also dependent on the cluster results. The initial estimate of the initial mixing proportion is $P(\boldsymbol{t}_{s_j} \in C_k)$. It is calculated by assuming that the clusters found using *k*-means clustering have a Gaussian distribution with mean $\boldsymbol{\mu}_{C_k}$ and covariance Σ_{C_k},

$$\Sigma_k = \Sigma_{C_k} \tag{14}$$

$$\alpha_k = P(\boldsymbol{t}_{s_j} \in C_k). \tag{15}$$

The parameters defining the K representative texture distributions are taken to be the mean and covariances for the K-estimated Gaussian distributions ($\hat{\boldsymbol{t}}_k^r = \boldsymbol{\mu}_k$). Furthermore, each texture vector is assigned to belong to the distribution which maximizes the weighted probability $\alpha_k P(\boldsymbol{t}_{s_j} | \boldsymbol{\mu}_k, \Sigma_k)$. The number of clusters in *k*-means clustering or distributions in the Gaussian mixture model is 10, which is determined to best model the set of skin and lesion textures.

C. Summary of the TDLS Segmentation Algorithm

1) Convert the corrected image to the XYZ color space.
2) For each pixel s in image I, extract the texture vector $\boldsymbol{t}_s$ to obtain the set of texture vectors $\mathcal{T}$ (1).
3) Cluster the texture vectors in $\mathcal{T}$, as described in Section IV-B, to obtain the representative texture distributions.
4) Calculate probability that two texture distributions are distinct $d_{j,k}$ using (6) for all possible pairs of texture distributions.
5) Calculate the textural distinctiveness metric D_j (7) for each texture distribution.
6) Apply the SRM algorithm to find the initial regions.
7) Calculate the region distinctiveness metric $\mathcal{D}_R$ for each initial region using (9).
8) Calculate the threshold τ between the normal skin and lesion classes (10).
9) Classify each region as normal skin or lesion based on the results of steps 7 and 8 (8).
10) Apply a morphological dilation operator to the initial lesion classification.
11) For each contiguous region in the initial segmentation, count the number of pixels in the region.

12) As the final lesion segmentation, return the contiguous region consisting of the most pixels.

V. Experimental Results

Two experiments are performed to compare the TDLS algorithm to other state-of-the-art algorithms. In the first experiment, the first step of the TDLS step, calculating the TD metric, is compared to a similar algorithm. The compared algorithm calculates a TD metric, but does not include statistical information. The second experiment compares the segmentation results obtained using the TDLS algorithm with four other segmentation algorithms designed for skin lesion images. The TDLS algorithm is implemented in MATLAB on a computer with an Intel Core i5-2400s CPU (2.5 GHz, 6-GB RAM). To segment a skin lesion in a 1640×1043 image, the algorithm has an average runtime of 62.45 s.

A. TD Comparison

The first step of the TDLS algorithm is compared to the results from the algorithm by Scharfenberger *et al.* [32], which calculates a similar TD metric and is referred to as the TD algorithm. The difference between the two algorithms is that the TDLS algorithm introduces the use of probabilistic information to determine representative texture distributions and to measure TD. To determine if incorporating this information is useful, TD maps produced using the first step of the TDLS algorithm are compared to distinctiveness maps produced using the TD algorithm. The TD algorithm only uses the k-means clustering algorithm to find the representative texture distributions. Furthermore, the TD algorithm does not take into account the covariance corresponding to each cluster when calculating the distinctiveness metric. Finally, because the TD algorithm is designed to compute saliency maps, the distinctiveness metric includes an additional term based on the distance between a pixel and the center of the image. Since we are interested in understanding the effect of the additional probabilistic information, this term was omitted in the comparisons.

The TD maps are compared visually. Select skin lesion images from the Dermquest database [40] are used for comparison, after being corrected for illumination variation using the MSIM algorithm [14]. These examples are selected because they highlight cases with significant differences between the TD and TDLS algorithms and are shown in Fig. 5. Also, the dynamic range of pixels is scaled to the maximum pixel intensity and minimum pixel intensity, resulting in a different dynamic range for each TD map.

Some interesting observations can be made from the examples. First, lesions in Fig. 5(a) and (c) are comprised of two distinct textures. For example, in Fig. 5(a), there are pronounced dark areas and lighter red areas. However, when using the TD algorithm, only the first texture is highlighted in the TD map. Using the TDLS algorithm, both textures are highlighted. This is also seen in Fig. 5(c).

As a tradeoff, distinct nonlesion areas that occur due to natural pigmentation and texture characteristics of the skin are also highlighted when using the TDLS algorithm. For example, in Fig. 5(a), the presence of shading on the left side of the image is highlighted when using the TDLS algorithm, but not when using the TD algorithm. This motivates use of the texture-based segmentation step in the TDLS algorithm, rather than using the textural distinctiveness maps directly.

B. Segmentation Comparison

The TDLS algorithm is compared to four state-of-the-art lesion segmentation algorithms. The first algorithm (L-SRM) is designed for dermatological images, but can be applied to lesion photographs as well. It applies the SRM algorithm outlined in Section III-A and uses the normal skin color to find the regions corresponding to the lesion. The three other algorithms are proposed by Cavalcanti *et al.* and are designed specifically for lesion photographs. One algorithm (Otsu-R) finds the Otsu threshold using the red color channel. The second (Otsu-RGB) uses all three RGB color channels and finds Otsu thresholds for each channel. The final algorithm (Otsu-PCA) processes the RGB color channels to find three more efficient channels to threshold. A texture channel is obtained using Gaussian filtering, a color channel is obtained using the inverse of the red color channel, and the third channel is found using PCA. For simplicity, this algorithm is referred to as Otsu-PCA. All algorithms have additional postprocessing steps to clean up the contour, and these steps have been implemented as described in their publication.

A set of 126 images from the Dermquest database [40] are used to test the segmentation algorithms. There are 66 photographs with lesions diagnosed as melanoma and 60brk photographs with lesions diagnosed as nonmelanoma. These images are selected because they satisfy the stated assumptions and can be adequately corrected for illumination variation. All tested photographs were first corrected using the MSIM algorithm [14]. The segmentation algorithms are compared to manually segmented ground truth. The algorithms are compared visually and by calculating sensitivity, specificity, and accuracy of the algorithm to properly classify each pixel as normal skin or lesion.

1) Visual Comparison: The objective of the visual comparison is to analyze the segmentation results qualitatively. Interesting examples of segmentation results are shown in Fig. 6, along with the ground truth. Many of these examples illustrate situations where existing state-of-the-art algorithms cannot accurately locate the lesion and the proposed algorithm can.

Fig. 6(a)–(f) is images of melanoma lesions, and Fig. 6(g) and (h) is nonmelanoma lesions. Fig. 6(a) and (b) correspond to the examples shown in Figs. 4 and 1.

Areas where illumination variation has not been fully corrected can be misclassified as part of the lesion, as seen in Fig. 6(c) and (g). In both those examples, there are uncorrected shadows which all algorithms except for the TDLS algorithm consider as part of the lesion. Complicated texture patterns in the skin area, as seen in Fig. 6(h), and artifacts such as hair, as seen in Fig. 6(e), are also often misclassified as part of the lesion. However, the TDLS algorithm is able to reasonably segment the lesion in those images.

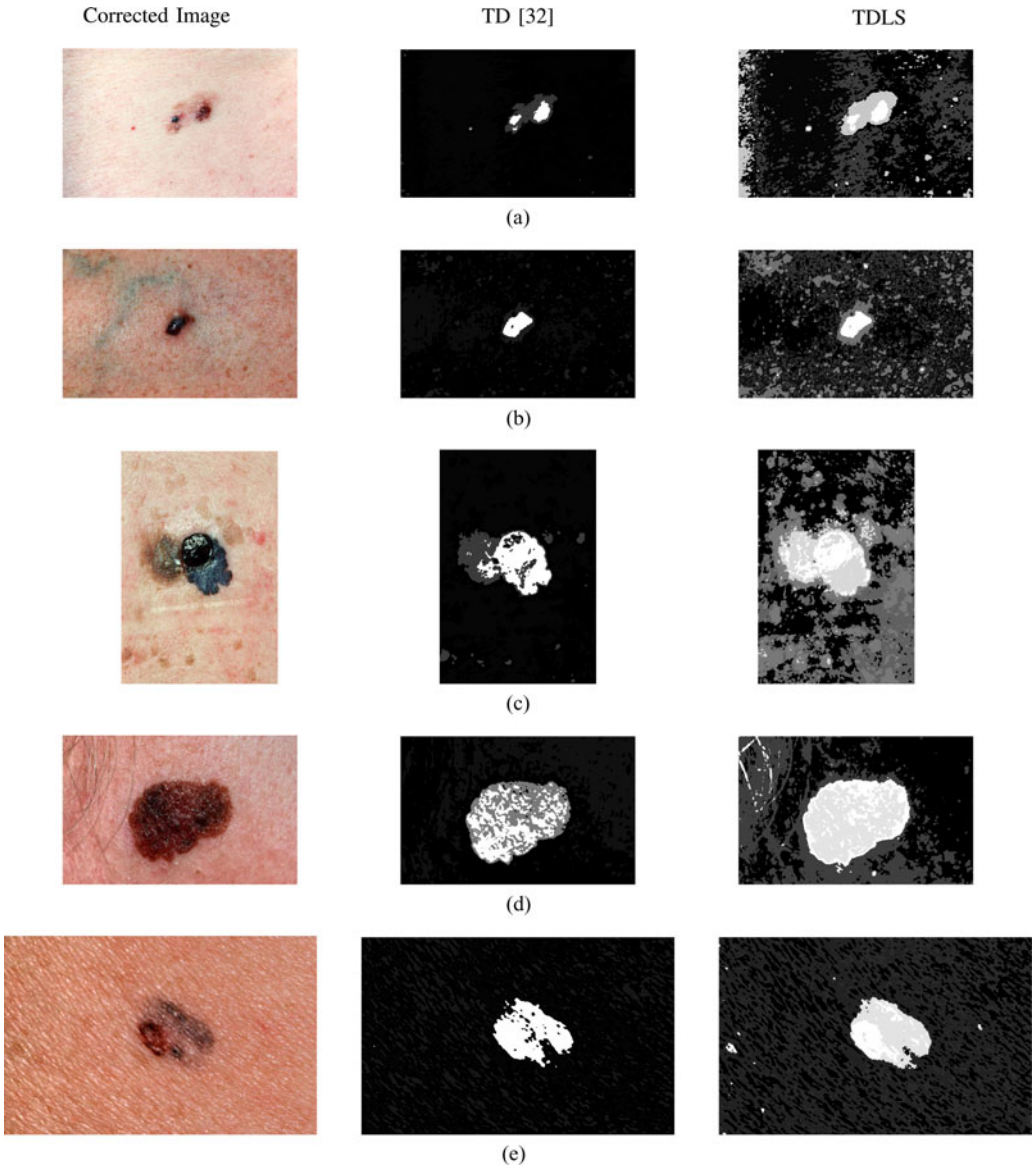

Fig. 5. Corrected skin lesion images and their corresponding textural distinctiveness maps. The textural distinctiveness maps are produced using the TD algorithm [32] and the first step of the TDLS algorithm. The pixel intensity corresponds to the TD of the pixel's associated texture distribution. The TDLS algorithm is able to better highlight the lesion area, compared to the TD algorithm. However, in (a) and (c), nonlesion areas are also highlighted by the TDLS algorithm.

Lesions can be comprised of different colors and textures, such as in Fig. 6(d) and (f). In fact, color variegation across a lesion is a feature that is used to classify lesions as melanoma. It is critical that segmentation algorithms can account for the color and texture variation when locating the skin lesion. The compared algorithms only find the most prominent color or texture and fail to include the subtler regions as part of the lesion. However, because the TDLS algorithm learns the lesion textures and normal skin textures, it is able to locate the entire lesion.

2) Segmentation Accuracy Comparison: The objective of this experiment is to measure sensitivity, specificity, and accuracy of each segmentation algorithm after the algorithms classify each pixel as belonging to the normal skin class or lesion class. Each algorithm is applied to the corrected images and the resulting segmentation is compared to the manually drawn segmentation acting as ground truth. The metrics used to compare to the ground truth are sensitivity, specificity, and accuracy. Their formulas are given in (16), (17), and (18), where TP is the number of true positive pixels, FP is the number of false positive pixels, TF is the number of true negative pixels, and FN is the number of false negative pixels,

$$\text{Sensitivity} = \frac{\text{TP}}{\text{TP} + \text{FN}} \tag{16}$$

$$\text{Specificity} = \frac{\text{TN}}{\text{TN} + \text{FP}} \tag{17}$$

$$\text{Accuracy} = \frac{\text{TP} + \text{TN}}{\text{TP} + \text{FN} + \text{TN} + \text{FP}}. \tag{18}$$

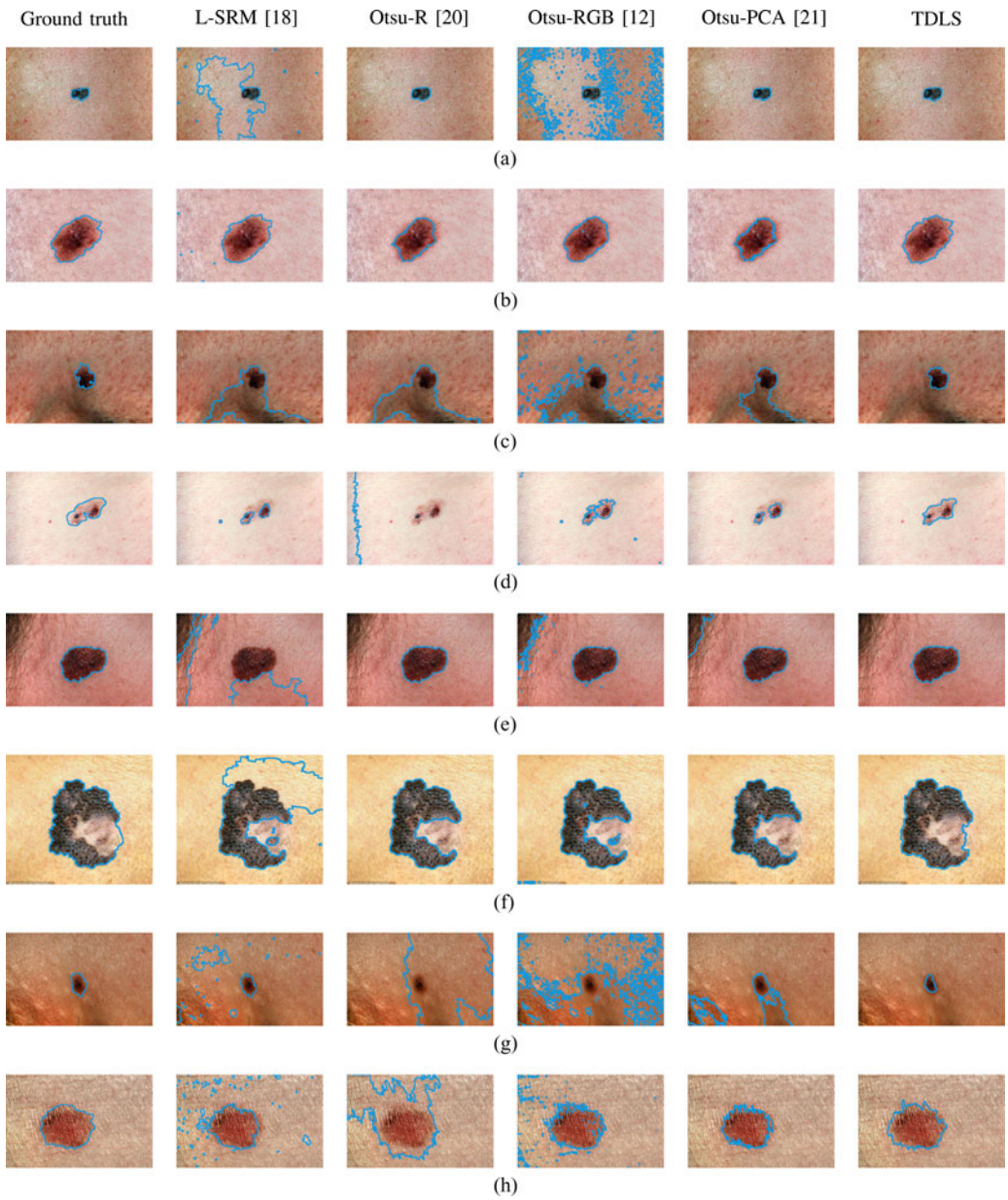

Fig. 6. Segmentation of skin lesions using various algorithms. In the first column, the manually segmented ground truth is shown. In the second to fifth columns, the results of state-of-the-art skin lesion segmentation algorithms are shown. The last column contains the results of the proposed TDLS algorithm.

TABLE I
SEGMENTATION ACCURACY RESULTS FOR ALL LESION PHOTOGRAPHS

Segmentation Algorithm	Sensitivity	Specificity	Accuracy
L-SRM [18]	89.4%	92.7%	92.3%
Otsu-R [20]	87.3%	85.4%	84.9%
Otsu-RGB [12]	**93.6%**	80.3%	80.2%
Otsu-PCA [21]	79.6%	**99.6%**	98.1%
TDLS	91.2%	99.0%	**98.3%**

TABLE II
SEGMENTATION ACCURACY RESULTS FOR MELANOMA LESION PHOTOGRAPHS

Segmentation Algorithm	Sensitivity	Specificity	Accuracy
L-SRM [18]	90.0%	92.5%	92.1%
Otsu-R [20]	87.4%	91.5%	90.3%
Otsu-RGB [12]	**92.2%**	85.5%	85.0%
Otsu-PCA [21]	81.2%	**99.5%**	97.6%
TDLS	90.8%	98.8%	**97.9%**

TABLE III
SEGMENTATION ACCURACY RESULTS FOR NONMELANOMA LESION PHOTOGRAPHS

Segmentation Algorithm	Sensitivity	Specificity	Accuracy
L-SRM [18]	88.7%	93.0%	92.6%
Otsu-R [20]	87.3%	78.7%	78.9%
Otsu-RGB [12]	**95.2%**	74.6%	75.0%
Otsu-PCA [21]	77.8%	**99.0%**	**98.7%**
TDLS	91.6%	99.1%	**98.7%**

Tables I, II, and III show the average sensitivity, specificity, and accuracy across the entire set of images or for just the melanoma or nonmelanoma photographs.

Table I shows that the TDLS algorithm has the highest accuracy across all tested photographs, followed closely by the Otsu-PCA algorithm. The TDLS algorithm also has the

second highest sensitivity and specificity. This trend follows when looking at subsets of melanoma or nonmelanoma photographs, as seen in Tables II and III. The Otsu-PCA algorithm has similar specificity and accuracy results, while the Otsu-RGB algorithm has better sensitivity. However, the TDLS algorithm is able to perform well in all three metrics.

VI. Conclusion

In summary, a novel lesion segmentation algorithm using the concept of TD is proposed. A probabilistic TD metric is introduced based on a learned model of normal skin and lesion textures. Representative texture distributions are learned from the image itself and the TD metric captures the dissimilarity between pairs of texture distributions. Then, the image is divided into numerous smaller regions and each of those regions are classified as lesion or skin based on the TD map. The entire proposed framework is tested by using the illumination corrected images as the input to the texture-based segmentation algorithm. It is compared to state-of-art lesion segmentation algorithms, including three algorithms designed for lesion images. The proposed framework produces the highest segmentation accuracy using manually segmented images as ground truth. A larger data collection and annotation process, including additional testing on a wide range of images, will be undertaken as future work. While the experimental results show that the proposed method is able to segment the lesion in images of different scales and levels of quality, it is worth conducting a more comprehensive analysis on the impact of image quality and scale on the proposed method.

References

[1] N. Howlader, A. M. Noone, M. Krapcho, J. Garshell, N. Neyman, S. F. Altekruse, C. L. Kosary, M. Yu, J. Ruhl, Z. Tatalovich, H. Cho, A. Mariotto, D. R. Lewis, H. S. Chen, E. J. Feuer, and K. A. Cronin, "SEER cancer statistics review, 1975-2010," Nat. Cancer Inst., Bethesda, MD, USA, Tech. Rep., 2013

[2] A. F. Jerants, J. T. Johnson, C. D. Sheridan, and T. J. Caffrey, "Early detection and treatment of skin cancer," *Amer. Family Phys.*, vol. 62, no. 2, pp. 1–6, Jul. 2000.

[3] Public Health Agency of Canada. (2013). Melanoma skin cancer. [Online]. Available:http://www.phac-aspc.gc.ca/cd-mc/cancer/melanoma_skin_cancer-cancer_peau_melanome-eng.php

[4] A. Jemal, M. Saraiya, P. Patel, S. S. Cherala, J. Barnholtz-Sloan, J. Kim, C. L. Wiggins, and P. A. Wingo, "Recent trends in cutaneous melanoma incidence and death rates in the united states, 1992-2006," *J. Amer. Acad. Dermatol.*, vol. 65, no. 5, pp. S17.e1–S17.e11, Nov. 2011.

[5] K. A. Freedberg, A. C. Geller, D. R. Miller, R. A. Lew, and H. K. Koh, "Screening for malignant melanoma: A cost-effectiveness analysis," *J. Amer. Acad. Dermatol.*, vol. 41, no. 5, pt. 1, pp. 738–745, Nov. 1999.

[6] M. E. Celebi, H. A. Kingravi, B. Uddin, H. Iyatomi, Y. A. Aslandogan, W. V. Stoecker, and R. H. Moss, "A methodological approach to the classication of dermoscopy images," *Comput. Med. Imag. Graph.*, vol. 31, no. 6, pp. 362–373, Sep. 2007.

[7] S. W. Menzies, L. Bischof, H. Talbot *et al.*, "The performance of solarscan: An automated dermoscopy image analysis instrument for the diagnosis of primary melanoma," *Archives Dermatol.*, vol. 141, no. 11, pp. 1388–1396, Nov. 2005.

[8] H. Iyatomi, H. Oka, M. E. Celebi, M. Hashimoto, M. Hagiwara, M. Tanaka, and K. Ogawa, "An improved internet-based melanoma screening system with dermatologist-like tumor area extraction algorithm," *Comput. Med. Imag. Graph.*, vol. 32, no. 7, pp. 566–579, Oct 2008.

[9] H. Ganster, A. Pinz, R. Rohrer, E. Wildling, M. Binder, and H. Kittler, "Automated melanoma recognition," *IEEE Trans. Med. Imag.*, vol. 20, no. 3, pp. 233–239, Mar. 2001.

[10] H. Iyatomi, M. Celebi, G. Schaefer, and M. Tanaka, "Automated color calibration method for dermoscopy images," *Comput. Med. Imag. Graph.*, vol. 35, no. 2, pp. 89–98, Mar. 2011.

[11] H. C. Engasser and E. M. Warshaw, "Dermatoscopy use by US dermatologists: A cross-sectional survey," *J. Amer. Acad. Dermatol.*, vol. 63, no. 3, pp. 412–419, 2010.

[12] P. G. Cavalcanti and J. Scharcanski, "Automated prescreening of pigmented skin lesions using standard cameras," *Comput. Med. Imag. Graph.*, vol. 35, no. 6, pp. 481–491, Sep. 2011.

[13] J. Alcon, C. Ciuhu, W. ten Kate, A. Heinrich, N. Uzunbajakava, G. Krekels, D. Siem, and G. De Haan, "Automatic imaging system with decision support for inspection of pigmented skin lesions and melanoma diagnosis," *IEEE J. Sel. Topics Signal Process.*, vol. 3, no. 1, pp. 14–25, Feb. 2009.

[14] J. Glaister, R. Amelard, A. Wong, and D. A. Clausi, "MSIM: Multi-stage illumination modeling of dermatological photographs for illumination-corrected skin lesion analysis," *IEEE Trans. Biomed. Eng.*, vol. 60, no. 7, pp. 1873–1883, Jul. 2013.

[15] R. J. Friedman, D. S. Rigel, and A. W. Kopf, "Early diagnosis of cutaneous melanoma: Revisiting the ABCD criteria," *CA: A Cancer J. Clinicians*, vol. 35, no. 3, pp. 130–151, May 1985.

[16] M. Celebi, H. Iyatomi, G. Schaefer, and W. V. Stoecker, "Lesion border detection in dermoscopy images," *Comput. Med. Imag. Graph.*, vol. 33, no. 2, pp. 148–153, 2009.

[17] B. Erkol, R. H. Moss, R. Joe Stanley, W. V. Stoecker, and E. Hvatum, "Automatic lesion boundary detection in dermoscopy images using gradient vector flow snakes," *Skin Res. Technol.*, vol. 11, no. 1, pp. 17–26, 2005.

[18] M. E. Celebi, H. A. Kingravi, H. Iyatomi, Y. A. Aslandogan, W. V. Stoecker, R. H. Moss, J. M. Malters, J. M. Grichnik, A. A. Marghoob, H. S. Rabinovitz, and S. W. Menzies, "Border detection in dermoscopy images using statistical region merging," *Skin Res. Technol.*, vol. 14, no. 3, pp. 347–353, 2008.

[19] G. Hance, S. Umbaugh, R. Moss, and W. Stoecker, "Unsupervised color image segmentation: with application to skin tumor borders," *IEEE Eng. Med. Biology Mag.*, vol. 15, no. 1, pp. 104–111, Jan./Feb. 1996.

[20] P. G. Cavalcanti, J. Scharcanski, and C. B. O. Lopes, "Shading attenuation in human skin color images," in *Advances in Visual Computing*, G. Bebis, R. Boyle, B. Parvin, D. Koracin, R. Chung, R. Hammoud, M. Hussain, T. Kar-Han, R. Crawfis, D. Thalmann, D. Kao, and L. Avila, Eds., (ser. Lecture Notes in Computer Science), vol. 6453 Heidelberg, Germany: Springer, 2010, pp. 190–198.

[21] P. Cavalcanti, Y. Yari, and J. Scharcanski, "Pigmented skin lesion segmentation on macroscopic images," in *Proc. 25th Int. Conf. Image Vision Comput. New Zealand.*, 2010, pp. 1–7.

[22] P. Cavalcanti, J. Scharcanski, L. Di Persia, and D. Milone, "An ICA-based method for the segmentation of pigmented skin lesions in macroscopic images," in *Proc. IEEE Annu. Int. Conf. Eng. Med. Biol. Soc.*, 2011, pp. 5993–5996.

[23] M. Anantha, R. H. Moss, and W. V. Stoecker, "Detection of pigment network in dermatoscopy images using texture analysis," *Comput. Med. Imag. Graph.*, vol. 28, no. 5, pp. 225–234, 2004.

[24] W. V. Stoecker, C.-S. Chiang, and R. H. Moss, "Texture in skin images: Comparison of three methods to determine smoothness," *Comput. Med. Imag. Graph.*, vol. 16, no. 3, pp. 179–190, 1992.

[25] A. P. Dhawan and A. Sim, "Segmentation of images of skin lesions using color and texture information of surface pigmentation," *Comput. Med. Imag. Graph.*, vol. 16, no. 3, pp. 163–177, 1992.

[26] M. Silveira, J. Nascimento, J. Marques, A. R. S. Marcal, T. Mendonca, S. Yamauchi, J. Maeda, and J. Rozeira, "Comparison of segmentation methods for melanoma diagnosis in dermoscopy images," *IEEE J. Sel. Topics Signal Process.*, vol. 3, no. 1, pp. 35–45, 2009.

[27] C. Serrano and B. Acha, "Pattern analysis of dermoscopic images based on Markov random fields," *Pattern Recog.*, vol. 42, no. 6, pp. 1052–1057, 2009.

[28] L. Xu, M. Jackowskia, A. Goshtasby, D. Roseman, S. Bines, C. Yu, A. Dhawan, and A. Huntley, "Segmentation of skin cancer images," *Image Vis. Comput.*, vol. 17, pp. 65–74, 1999.

[29] S. Hwang and M. E. Celebi, "Texture segmentation of dermoscopy images using Gabor filters and g-means clustering," in *Proc. Int. Conf. Image Process., Comput. Vision, Pattern Recog*, Jul. 2010, pp. 882–886.

[30] G. Peyre, "Sparse modeling of textures," *J. Math. Imag. Vis.*, vol. 34, no. 1, pp. 17–31, 2009.
[31] J.-L. Starck, M. Elad, and D. Donoho, "Image decomposition via the combination of sparse representations and a variational approach," *IEEE Trans. Image Process.*, vol. 14, no. 10, pp. 1570–1582, Oct. 2005.
[32] C. Scharfenberger, A. Wong, K. Fergani, J. S. Zelek, and D. A. Clausi, "Statistical textural distinctiveness for salient region detection in natural images," in *Proc. IEEE Conf. Comput. Vis. Pattern Recog.*, Jun. 2013, pp. 979–986.
[33] R. Nock and F. Nielsen, "Statistical region merging," *IEEE Trans. Pattern Anal. Mach. Intell.*, vol. 26, no. 11, pp. 1452–1458, Nov 2004.
[34] N. Otsu, "A threshold selection method from gray-level histograms," *IEEE Trans. Syst., Man, Cybern.*, vol. 9, no. 1, pp. 62–66, 1979.
[35] P. Soille, *Morphological Image Analysis: Principles and Applications Image Processing*, 2nd ed. ed. Berlin, Germany: Springer, 2003.
[36] J.-C. Terrillon, M. Shirazi, H. Fukamachi, and S. Akamatsu, "Comparative performance of different skin chrominance models and chrominance spaces for the automatic detection of human faces in color images," in *Proc. 4th IEEE Int. Conf. Autom. Face Gesture Recog.*, 2000, pp. 54–61.
[37] A. K. Jain, R. P. W. Duin, and J. Mao, "Statistical pattern recognition: a review," *IEEE Tran. Pattern Anal. Mach. Intell.*, vol. 22, no. 1, pp. 4–37, Jan 2000.
[38] M. Celebi, H. Kingravi, and P. A. Vela, "A comparative study of efficient initialization methods for the k-means clustering algorithm," *Expert Syst. Appl.*, vol. 40, no. 1, pp. 200–210, Sep. 2012.
[39] M. A. T. Figueiredo and A. K. Jain, "Unsupervised learning of finite mixture models," *IEEE Trans. Pattern Anal. Mach. Intell.*, vol. 24, no. 3, pp. 381–396, Mar. 2002.
[40] DermQuest, (2012). [Online]. Available:http://www.dermquest.com

Jeffrey Glaister (S'12) received the B.A.Sc. degree in systems design engineering in 2011 and the M.A.Sc. degree in systems design engineering in 2013, both from the University of Waterloo, Waterloo, ON, Canada. He is currently working toward the Ph.D. degree in electrical and computer engineering at Johns Hopkins University, Baltimore, MD, USA.

He is a member of the Image Analysis and Communications lab, Johns Hopkins University. His current research topic is parcellation of thalamic nuclei from magnetic resonance images and past research included segmentation of skin lesions from dermatological photographs. His research interests include biomedical image processing, remote sensing, and pattern recognition.

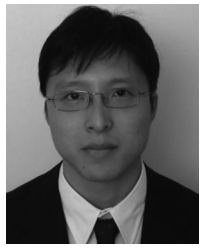

Alexander Wong (M'05) received the B.A.Sc. degree in computer engineering, the M.A.Sc. degree in electrical and computer Engineering, and the Ph.D. degree in systems design engineering from the University of Waterloo, Waterloo, ON, Canada, in 2005, 2007, and 2010 respectively. He is currently the Canada Research Chair in Medical Imaging Systems and an Assistant Professor in the Department of Systems Design Engineering, University of Waterloo. He has published refereed journal and conference papers, as well as patents, in various fields such as computer vision, graphics, image processing, multimedia systems, and wireless communications. His research interests include image processing, computer vision, pattern recognition, and cognitive radio networks, with a focus on biomedical and remote sensing image processing and analysis such as image registration, image denoising and reconstruction, image superresolution, image segmentation, tracking, and image, and video coding and transmission.

Dr. Wong received an Outstanding Performance Award, an Engineering Research Excellence Award, an Early Researcher Award from the Ministry of Economic Development and Innovation, a Best Paper Award by the Canadian Image Processing and Pattern Recognition Society, and the Alumni Gold Medal.

David A. Clausi (S'93–M'96–SM'03) received the Ph.D. degree in systems design engineering at the University of Waterloo, Waterloo, ON, Canada, in 1996.

He then worked in software medical imaging at AGFA, Waterloo. He started his academic career in 1997 as an Assistant Professor in Geomatics Engineering at the University of Calgary, Calgary, AB, Canada. In 1999, he returned to his alma mater and is currently a Professor specializing in the fields of Intelligent and Environmental Systems and recently became the Associate Chair for graduate studies. He is an active interdisciplinary and multidisciplinary Researcher. He has an extensive publication record, publishing refereed journal and conference papers in the diverse fields of remote sensing, computer vision, algorithm design, and biomechanics. His research efforts have led to successful commercial implementations including creating, building, and selling his own company.

Dr. Clausi was the Co-chair of IAPR Technical Committee 7 Remote Sensing during 2004–2006. He has received numerous scholarships, paper awards, and two Teaching Excellence Awards. In 2010, he received the award for Research Excellence and Service to the Research Community by the Canadian Image Processing and Pattern Recognition Society.